A Unified Force Controller for a Proportional-Injector Direct-Injection Monopropellant-Powered Actuator

Kevin B. Fite, Jason E. Mitchell, Eric J. Barth, and Michael Goldfarb

Department of Mechanical Engineering
Vanderbilt University, Nashville, TN 37235

Version: *September 8, 2005*

To appear in the
ASME Journal of Dynamic Systems, Measurement, and Control, vol. 128, no. 3, 2006.

Abstract

This paper describes the modeling and control of a proportional-injector direct-injection monopropellant powered actuator for use in power-autonomous human-scale mobile robots. The development and use of proportional (as opposed to solenoid) injection valves enables a continuous and unified input/output description of the device, and therefore enables the development and implementation of a sliding-mode-type controller for the force control of the proposed actuator that provides the stability guarantees characteristic of a sliding mode control approach. Specifically, a three-input, single-output model of the actuation system behavior is developed, which takes a nonlinear non-control-canonical form. In order to implement a nonlinear controller, a constraint structure is developed that effectively renders the system single-input, single-output and control canonical, and thus of appropriate form for the implementation of a sliding mode controller. A sliding mode controller is then developed and experimentally implemented on the proposed actuator. Experimental results demonstrate closed loop force tracking with a saturation-limited bandwidth of approximately 6 Hz.

1 Introduction

Energetic deficiencies in state-of-the-art power supply and actuation limit significantly the utility of human-scale self-powered robots (see, for example, discussion in [1]). Such deficiencies have motivated the development of alternative actuators that have the potential to deliver improved energetic characteristics relative to battery-powered servomotors. Specifically, Goldfarb et al. and Shields et al. have proposed two types of liquid-monopropellant-powered actuators, a centralized and a direct-injection type, respectively, that provide the promise of significantly improved energetic properties relative to battery-powered servomotors [1, 2]. Such liquid-fueled actuators represent an enabling technology for the existence of a wide range of power autonomous human-scale mobile robot platforms with useful operating times and significant output work capabilities. Though monopropellants have been utilized in thrusters in numerous aerospace applications (see, for example, [3-5]), and recently as the power source for a free piston hydraulic pump [6], little prior work exists regarding their use in servo-controlled actuators. The first appearance of such work, described by Goldfarb et al. [1], is much like a standard pneumatic actuation system, but utilizes a monopropellant gas generator in place of an air compressor. This configuration incorporates a solenoid valve to meter the flow of hydrogen peroxide through a catalyst pack and into a high-pressure hot gas reservoir. Like a conventional pneumatic actuation system, a four-way proportional spool valve controls the flow of compressible fluid (in this case a hot gas) from the reservoir into one side of a pneumatic piston while exhausting the other side to atmosphere. The servocontrol of this system is therefore nearly identical to a standard pneumatic servosystem, and as such, a standard control approach was used (i.e., a full-

state-feedback position-velocity-acceleration controller). As in most fluid-powered actuators, high-bandwidth control of power is achieved via dissipative means (i.e., the gas flow is throttled via a servovalve), which can significantly decrease the efficiency of energy conversion. Rather than use a servovalve to modulate a high-power gas flow, the configuration described by Shields et al. [2] uses solenoid valves to modulate the (low power) flow of liquid propellant, and thus essentially eliminates power losses due to fluid throttling (i.e., the fuel flow rates are orders of magnitude lower than the gas flow rates, and as such, control losses are essentially eliminated). Unlike the configuration described in [1], control of the actuator described in [2] is considerably more complex, and as such, the bulk of the work described in [2] is the control methodology by which the proposed solenoid-injected direct-injection actuator is controlled. Though the control approach presented in [2] works effectively, its mixed discrete/continuous nature (i.e., discrete injection, proportional exhaust) requires assumptions of model linearity, and the approach utilized provides relative weak stability guarantees. The work presented herein is an effort to develop a unified nonlinear controller for an actuator similar to that presented in [2], that additionally provides asymptotic stability guarantees. In order to do so, proportional injector valves were developed, which were not otherwise commercially available. By incorporating these proportional injector valves in place of the solenoid valves utilized in [2], the system retains its energetic advantages (i.e., throttles liquid rather than gas, and thus entails negligible energy dissipation), but provides an input/output model that, after some manipulation, is appropriate for nonlinear sliding mode control. The resulting controller takes advantage of the full nonlinear model, and provides the asymptotic stability guarantees of the sliding mode structure. Thus, this

paper derives a unified model of the actuator; manipulates the model to obtain a single-input, single-output control canonical form; implements a sliding mode controller based on this modified form; and finally, experimentally demonstrates the controller on an actuator prototype.

2 PIDI Actuator Prototype

Figure 1 depicts a schematic of the proportional-injector direct-injection (PIDI) actuator prototype. The actuation system consists of two proportional injection valves and one proportional exhaust valve, which together control the flow into and out of opposing sides of a hot-gas cylinder. Specifically, liquid monopropellant is stored in a blowdown propellant tank, which is pressurized by an inert gas. The liquid monopropellant is proportionally metered by the injection valves through catalyst packs, where it is catalyzed into hot gas, and injected into the respective sides of the cylinder. A three-way proportional hot-gas exhaust valve controls the flow of gas leaving each chamber of the actuator. Though pneumatic cylinders capable of operating at the desired hot gas temperatures are commercially available, neither the appropriate proportional injection valves nor the three-way exhaust valve are commercially available. As such, the authors designed and fabricated these valves for the proposed PIDI actuator. A prototype of the PIDI actuator, with the aforementioned valves, is shown mounted on a single-degree-of-freedom robot arm in Fig. 2. The system consists of the monopropellant fuel tank, the PIDI actuator, the robot arm (shown holding an 11.2 kg mass), pressure sensors to measure the cylinder chamber pressures, and an encoder and tachometer to provide arm (and cylinder) position and velocity feedback.

3 Actuator Model

A detailed schematic of the PIDI actuator is shown in Fig. 3. Implementation of model-based force control requires a description of the dynamics from the (three) valve inputs (valve orifice areas: $A_{v,A}$, $A_{v,B}$, $A_{v,ex}$) to the actuator force output (F_{act}). The output force of the hot-gas cylinder is given by:

$$F_{act} = P_A A_A - P_B A_B + P_{atm} A_r \tag{1}$$

where P_A and P_B are the pressures in chambers A and B, respectively, A_A and A_B are the cross-sectional areas of chambers A and B, respectively, P_{atm} is atmospheric pressure, and A_r is the cross-sectional area of the piston rod. Assuming an adiabatic process, the pressures in each chamber are governed by:

$$\dot{P}_A + \frac{\gamma \dot{V}_A}{V_A} P_A = \frac{\gamma R T_{ADT}}{V_A} (\dot{m}_{in,A} - \dot{m}_{out,A}) \tag{2}$$

$$\dot{P}_B + \frac{\gamma \dot{V}_B}{V_B} P_B = \frac{\gamma R T_{ADT}}{V_B} (\dot{m}_{in,B} - \dot{m}_{out,B}) \tag{3}$$

where V_A and V_B are the volumes in each cylinder chamber, γ is the ratio of specific heats of the gas, R is the specific gas constant, T_{ADT} is the adiabatic decomposition temperature of the monopropellant, and $\dot{m}_{in,A}$, $\dot{m}_{out,A}$, $\dot{m}_{in,B}$ and $\dot{m}_{out,B}$ are the mass flow rates of gas into or out of each cylinder chamber. Note that the right-hand-side of Eqs. (2) and (3) implicitly assume that the dependence of the enthalpy term on the rate of change of temperature is small. The mass flow rate terms in the pressure dynamics of Eqs. (2) and (3) take one of two forms, depending upon whether the cylinder chamber is being injected ($\dot{m}_{in}$), or exhausted ($\dot{m}_{out}$).

A. Injection Form

The injection form of the mass flow rate is a filtered version of the valve area command, filtered by the catalytic reaction dynamics. Specifically, if heat loss in the catalyst pack is neglected and the stored internal energy assumed small, the heat release from the catalytic decomposition directly results in enthalpy generation and the mass flow rate of compressible gas leaving the catalyst pack (and entering the gas cylinder) is given by:

$$\dot{m}_{in} = \frac{\dot{Q}_r}{c_p \widetilde{T}} \tag{4}$$

where c_p is the specific heat at constant pressure, $\dot{Q}_r$ is the rate of heat production in the catalyst pack, and $\widetilde{T}$ is a reference temperature associated with the reaction defined by the ratio of the lower heating value of the propellant to the specific heat at constant pressure of the reaction products (i.e., defined to preserve mass continuity through the catalyst pack). As experimentally shown in [8], the heat produced by the catalyst pack can be described by a first order dynamic in response to inlet propellant mass flow rate as:

$$\tau_r \ddot{Q}_r + \dot{Q}_r = k\dot{m}_{fuel} \tag{5}$$

where $\dot{m}_{fuel}$ is the mass flow rate of propellant entering the catalyst pack, τ_r is the (experimentally determined) reaction time constant, and k is the lower heating value of the propellant. A theoretical model presented in [9] further verifies the experimentally measured dynamic associated with the decomposition rate, associating the first-order response to the Arrhenius Law. The mass flow rate of liquid propellant through the injection valve can be described by assuming turbulent flow as follows:

$$\dot{m}_{fuel} = cA_v\sqrt{2\rho_L(P_s - P)} \tag{6}$$

where c is the (experimentally determined) discharge coefficient of the liquid fuel valve, A_v is the inlet orifice area of the liquid fuel valve (i.e., the injection valve command), ρ_L is the density of the liquid monopropellant, P_s is the supply pressure in the blowdown tank, and P is the downstream pressure. Combining Eqs. (4)-(6), the injection form of the mass flow input can be written as a function of the injection valve command as:

$$\tau_r\dot{\dot{m}}_{in} + \dot{m}_{in} = cA_v\sqrt{2\rho_L(P_s - P)} \tag{7}$$

B. Exhaust Form

Unlike the injection form of the mass flow rate, the exhaust form is algebraically related to the valve command, as described by standard equations for the isentropic flow of an ideal gas through a converging nozzle. Specifically, the exhaust mass flow rate for a given cylinder chamber is given by:

$$\dot{m}_{out} = \Psi(P)\,\mathrm{sgn}(A_{v,ex})A_{v,ex} \tag{8}$$

where $A_{v,ex}$ is the orifice area (of the exhaust valve) between the respective cylinder and atmosphere, and $\Psi(P)$ is an algebraic function of cylinder pressure, given by:

$$\Psi(P) = \begin{cases} \dfrac{C_1 C_f P}{\sqrt{T}} & \text{if } \dfrac{P_{atm}}{P} \le C_r \text{ (choked)} \\ \dfrac{C_2 C_f P}{\sqrt{T}}\left(\dfrac{P_{atm}}{P}\right)^{(1/k)}\sqrt{1-\left(\dfrac{P_{atm}}{P}\right)^{(k-1)/k}} & \text{otherwise (unchoked)} \end{cases} \tag{9}$$

where C_f is the discharge coefficient of the exhaust valve, C_r is the critical ratio governing the transition between subsonic and sonic flow, and C_1 and C_2 are constants defined by:

$$C_1 = \sqrt{\frac{\gamma}{R}\left(\frac{2}{\gamma+1}\right)^{\left(\frac{\gamma+1}{\gamma-1}\right)}} \tag{10}$$

$$C_2 = \sqrt{\frac{2\gamma}{R(\gamma-1)}} \tag{11}$$

C. System Dynamics

Note that, while the exhaust valve input shows up directly in the mass flow rate, as described by Eq. (8), the injection valve input shows up in the first derivative of mass flow rate, as described by Eq. (7). As such, the exhaust valve command first appears in the first derivative of output force, while the injection valve command first appears in the second derivative of the output force. Combining Eqs. (1) through (11), the dynamics of the PIDI actuator with all inputs can thus be expressed as:

$$\ddot{F}_{act} = \ddot{P}_A A_A - \ddot{P}_B A_B \tag{12}$$

where

$$\begin{aligned}\ddot{P}_{(A,B)} = {} & \frac{\gamma R T_{ADT}}{V_{(A,B)}}\left(\ddot{m}_{in} - \ddot{m}_{out}\right)_{(A,B)} - \frac{\gamma R T_{ADT}\dot{V}_{(A,B)}}{V^2{}_{(A,B)}}\left(\dot{m}_{in} - \dot{m}_{out}\right)_{(A,B)} \\ & - \frac{\gamma}{V_{(A,B)}}\left(P\ddot{V} + \dot{P}\dot{V} - \frac{P\dot{V}^2}{V}\right)_{(A,B)}\end{aligned} \tag{13}$$

and where $\ddot{m}_{in(A,B)}$ and $\dot{m}_{in(A,B)}$ are algebraic and filtered versions, respectively, of $A_{v,A}$ and $A_{v,B}$, as described by Eq. (7), while $\ddot{m}_{out(A,B)}$ and $\dot{m}_{out(A,B)}$ are differentiated and algebraic versions, respectively, of $A_{v,ex}$, as described by Eqs. (8)-(11). Note finally that $A_{v,A}$ and $A_{v,B}$ are one-sided control commands (i.e., positive only), while $A_{v,ex}$ is a signed area, such that a positive quantity corresponds to exhausting chamber *B*, while a negative quantity corresponds to exhausting chamber *A*.

4 Nonlinear Model-Based Control

Application of many standard nonlinear control techniques requires that the dynamics be expressed in a control canonical form, where all the inputs appear (algebraically) in the highest order state equation, and there exists a single input for each output (i.e., a square system). The dynamics of the PIDI monopropellant-powered actuator deviate from a control canonical form in two significant ways. First, the highest order equation contains both control inputs and integrated or differentiated versions of those inputs (injection and exhaust commands, respectively). Second, the system is not square, since the single (force) output is influenced by three (valve) inputs. In order to implement a standard nonlinear control approach such as sliding mode control, a constraint structure is developed that renders the system control canonical and square.

A. Anti-symmetric Valve Constraint

The first constraint imposed on the actuator disallows the simultaneous injection and exhaust of any given cylinder chamber. Specifically, if one chamber is being injected, then the opposite must be exhausted. As such, two modes of operation exist, one corresponding to a positive control effort (i.e., the charging of chamber *A* and discharging of chamber *B*) and the other corresponding to a negative control effort (i.e., the discharging of chamber *A* and charging of chamber *B*). Thus, the two unsigned and one signed valve commands can be expressed in terms of two signed intermediate control variables as follows:

$$\text{Positive control effort}: \begin{cases} A_{v,A} = u_{in} \\ A_{v,B} = 0 \\ A_{v,ex} = u_{out} \geq 0 \end{cases} \quad \text{for } u_{in} \geq 0 \tag{14}$$

$$\text{Negative control effort}: \begin{cases} A_{v,A} = 0 \\ A_{v,B} = -u_{in} \\ A_{v,ex} = u_{out} < 0 \end{cases} \quad \text{for } u_{in} < 0 \tag{15}$$

where u_{in} and u_{out} are the two signed intermediate control inputs. Thus, introduction of the anti-symmetric valve constraint renders the PIDI dynamics a two-input, single-output system.

B. Anti-symmetric Pressure Rate Constraint

The two intermediate control inputs can be dynamically related by constraining the desired rate of depressurization in the exhausting cylinder chamber to be equal to the rate of pressurization in the opposing injecting chamber, such that:

$$\text{Positive control}: \quad \dot{P}_{B,d} = -\dot{P}_A \tag{16}$$

$$\text{Negative control}: \quad \dot{P}_{A,d} = -\dot{P}_B \tag{17}$$

where $\dot{P}_{(A,B),d}$ is the desired rate of pressurization of the exhausting chamber for a given mode, and $\dot{P}_{(A,B)}$ is the actual rate of pressurization of the injecting chamber for a given mode. The constraints expressed by Eqs. (16) and (17) can be used along with the system dynamics to relate the outlet mass flow rate to the inlet flow rate, which after manipulation can be used to relate the two intermediate control variables. Specifically, using Eqs. (2-3) and Eqs. (16-17), the outlet mass flow can be expressed as:

$$\dot{m}_{out} = \frac{V_{ex}}{RT_{ADT}} \left(\frac{P_A \dot{V}_A}{V_A} + \frac{P_B \dot{V}_B}{V_B} \right) - \frac{V_{ex}}{V_{in}} \dot{m}_{in} \tag{18}$$

where V_{ex} and P_{ex} are the exhaust-side chamber volume and pressure, respectively, and V_{in} is the injection-side chamber volume. Combining Eqs. (18) with (8), the intermediate

control variable u_{out} can be related to the inlet mass flow rate by:

$$u_{out} = \frac{V_{ex}}{\Psi(P_{ex})RT_{ADT}}\left(\frac{P_A\dot{V}_A}{V_A} + \frac{P_B\dot{V}_B}{V_B}\right) - \frac{V_{ex}}{\Psi(P_{ex})V_{in}}\dot{m}_{in} \tag{19}$$

The inlet mass flow rate is simply a filtered version of the intermediate control variable u_{in} as given by Eq. (7). As such, the combination of Eqs. (19) and (7) yields a solution for u_{out} as a function of u_{in}, where u_{out} is a nonlinear filtered version of the intermediate control input u_{in}. Therefore, all inputs in the PIDI actuator can be derived from the single intermediate control variable u_{in}. The system is now a single-input, single-output system in control canonical form, to which a standard model-based nonlinear control approach can be applied.

C. Sliding Mode Control

The dynamics of the PIDI monopropellant-powered actuator are now expressible in a single-input, single-output nonlinear control canonical form, to which a sliding mode control design method can be applied. The actuator force dynamics expressed by Eqs. (14-15), which were previously a function of three control inputs, are now expressed in the general form as a function of u_{in} as follows:

$$\ddot{F}_{act} = f_{act}(\mathbf{x}) + b_{act}(\mathbf{x})u_{in} \tag{20}$$

where

$$f_{act}(\mathbf{x}) = [A_{(A,B)}f_{in}(\mathbf{x}) - A_{(B,A)}f_{ex}(\mathbf{x})]\,\mathrm{sgn}(u_{in}) \tag{21}$$

and

$$b_{act}(\mathbf{x}) = [A_{(A,B)}b_{in}(\mathbf{x}) - A_{(B,A)}b_{ex}(\mathbf{x})]\,\mathrm{sgn}(u_{in}) \tag{22}$$

where

$$f_{in}(\mathbf{x}) = \frac{-\gamma RT_{ADT}}{V_{in}}\left(\frac{1}{\tau_r} + \frac{\dot{V}_{in}}{V_{in}}\right)\dot{m}_{in} + \gamma\left(-\frac{\dot{P}_{in}\dot{V}_{in} + P_{in}\ddot{V}_{in}}{V_{in}} + \frac{P_{in}\dot{V}_{in}^2}{V_{in}^2}\right) \tag{23}$$

and

$$\begin{aligned} f_{ex}(\mathbf{x}) = {} & \frac{2\gamma RT_{ADT}}{\pi V_{ex}}\left(-\dot{\Psi}(P_{ex})\bar{u}_{out}\tan^{-1}\left(\frac{-\dot{m}_{out}}{\Psi(P_{ex})\bar{u}_{out}}\right)\right) \\ & + \frac{2\gamma RT_{ADT}}{\pi V_{ex}}\left(f_{\dot{m}_d}(\mathbf{x}) - \frac{\dot{m}_{out}\dot{\Psi}(P_{ex})}{\Psi(P_{ex})}\right)\left(1 + \left(\frac{\dot{m}_{out}}{-\Psi(P_{ex})\bar{u}_{out}}\right)^2\right)^{-1} \\ & + \gamma\left(-\frac{\dot{P}_{ex}\dot{V}_{ex} + P_{ex}\ddot{V}_{ex}}{V_{ex}} + \frac{P_{ex}\dot{V}_{ex}^2}{V_{ex}^2}\right) \end{aligned} \tag{24}$$

where

$$\begin{aligned} f_{\dot{m}_d}(\mathbf{x}) = {} & \left(\frac{V_{ex}}{\tau_r V_{in}} - \frac{\dot{V}_{ex}}{V_{in}} + \frac{\dot{V}_{in}V_{ex}}{V_{in}^2}\right)\dot{m}_{in} + \frac{\dot{V}_{ex}}{RT_{ADT}}\left(\frac{P_A\dot{V}_A}{V_A} + \frac{P_B\dot{V}_B}{V_B}\right) \\ & + \frac{V_{ex}}{RT_{ADT}}\left(\frac{\dot{P}_A\dot{V}_A + P_A\ddot{V}_A}{V_A} - \frac{P_A\dot{V}_A^2}{V_A^2} + \frac{\dot{P}_B\dot{V}_B + P_B\ddot{V}_B}{V_B} - \frac{P_B\dot{V}_B^2}{V_B^2}\right) \end{aligned} \tag{25}$$

and

$$b_{in}(\mathbf{x}) = \frac{\gamma RT_{ADT}c\sqrt{2\rho_L(P_s - P_{in})}}{\tau_r V_{in}} \tag{26}$$

and

$$b_{ex}(\mathbf{x}) = -\frac{2}{\pi}\left(1 + \left(\frac{\dot{m}_{out}}{-\Psi(P_{ex})\bar{u}_{out}}\right)^2\right)^{-1} b_{in}(\mathbf{x}) \tag{27}$$

Based on the standard sliding mode control approach, the independent intermediate control command is given by:

$$u_{in} = u_{in,eq} - K\,\mathrm{sat}\left(\frac{s}{\Phi}\right) \tag{28}$$

where K and Φ are controller gains, s is given by:

$$s = \dot{F}_{act} - \dot{F}_{act,d} + \lambda(F_{act} - F_{act,d}) \tag{29}$$

where $F_{act,d}$ is the desired actuator force of the PIDI actuator and λ is a gain, and $u_{in,eq}$ is given by:

$$u_{in,eq} = \frac{1}{b_{act}(\mathbf{x})}\left[\ddot{F}_{act,d} - \lambda(\dot{F}_{act} - \dot{F}_{act,d}) - f_{act}(\mathbf{x})\right] \tag{30}$$

Based on the sliding mode computation of u_{in}, the dependent intermediate control command u_{out} is computed via Eqs. (19) and (7). Finally, based on these intermediate control variables, the respective valve area commands are given by Eqs. (14) or (15), depending on the direction of the control effort (i.e., on the sign of u_{in}).

5 Force Tracking Results

Simulation of the proposed actuator force control approach (not presented here) was followed by an experimental validation, performed on the prototype shown in Fig. 2. All tests were conducted using 70% hydrogen peroxide as a monopropellant. The parameters used in the model-based controller are given in Table 1. Based on these parameters, the actuator was commanded to follow a 200 N amplitude sinusoidal force trajectory of varying frequencies. During the tests, the robot arm was externally constrained by a human operator in a flexible manner (i.e., held with a moderate impedance) such that the arm could move around in its workspace, but could not reach its upper or lower position limits. Figure 4 shows the results of force tracking for a sinusoidal input command of 1 Hz, along with the corresponding valve commands. Note that, since each valve is a closed-loop controlled dynamic system, the valve commands (which are the outputs of the unified actuator controller) are shown with a dashed line, while the actual valve areas are shown with a solid line. As can be seen in the figure, the unified controller obtains control of the actuator force primarily by modulating the mass flow into and out of chamber *A* (i.e., modulating the pressure in chamber *A*), while holding chamber *B* at an

approximately constant pressure. Figure 5 shows the results of force tracking for a sinusoidal input command of 4 Hz, along with the corresponding valve commands. Unlike the 1 Hz tracking in Fig. 4, the controller actively incorporates both injection valves in order to achieve the desired force tracking, which enables a higher differential mass flow rate between chambers, and thus a greater achievable rate of differential pressurization and a greater rate of change of force. Note that the difference in controller "strategy" between the 1 Hz tracking (primarily modulating a single chamber) and the 4 Hz tracking (modulating both chambers) is not explicitly dictated, but implicit in the behavior of the unified controller. Figure 6 shows the results of force tracking for a sinusoidal input command of 6 Hz, which approximately captures the -3dB bandwidth of the actuator. Like the 4 Hz tracking in Fig. 5, the controller actively incorporates both injection valves in order to provide the desired force tracking. However, as seen in Fig. 6, a significant amount of phase lag exists between the unified controller output and the actual injection valve areas, which limits the ability of the actuator to track the desired force. Thus the closed-loop bandwidth of the PIDI actuator appears to be limited by the bandwidth of the injection valves.

6 Conclusions

This paper presents the design of a unified sliding mode force controller for a proportional injector direct-injection monopropellant-powered actuator for use in human-scale power-autonomous robots. A model of the actuator is developed, which takes a three-input, single-output, nonlinear non-control-canonical form. In order to implement a model-based sliding mode controller, a constraint structure is developed, through which

the system dynamics can be represented in single-input, single-output control canonical form. Using the reformulated form of the system dynamics, a sliding mode controller is developed, and experimentally shown to provide good force tracking performance.

References

[1] M. Goldfarb, E.J. Barth, M.A. Gogola, and J.A. Wehrmeyer, "Design and Energetic Characterization of a Liquid-Propellant-Powered Actuator for Self-Powered Robots," *IEEE/ASME Transactions on Mechatronics,* Vol. 8, No. 2, pp. 254-262, 2003.

[2] B. Shields, K. Fite, and M. Goldfarb, "Control of a Direct Injection Liquid Fueled Actuator", *Proceedings of the ASME International Mechanical Engineering Congress and Exposition*, IMECE2004-59442, 2004.

[3] H. C. Hearn, "Flight Performance of a High-Impulse Monopropellant Thruster", *Journal of Thermal Analysis and Calorimetry*, Vol. 59, pp. 901-911, 2000.

[4] D. C. Morrisey, "Historical Perspective. Viking Mars Lander Propulsion", *Journal of Propulsion and Power*, Vol. 8, No. 2, pp. 320-331, 1992.

[5] D. L. Hitt, C. M. Zakrzwski, and M. A. Thomas, "MEMS-based Satellite Mircopropulsion via Catalyzed Hydrogen Peroxide Decomposition", *Smart Materials and Structures*, Vol. 10, No. 6, pp. 1163-1175, 2001.

[6] T. G. McGee, J. W. Raade, and H. Kazerooni, "Monopropellant-driven Free Piston Hydraulic Pump for Mobile Robotic Systems", *ASME Journal of Dynamic Systems, Measurement, and Control*, Vol. 126, No. 1, pp. 75-81, 2004.

[7] K. Fite, J. Mitchell, M. Goldfarb, and E.J. Barth, "Design and Characterization of a High-Bandwidth Rotary Hot Gas Valve," *Proceedings of the ASME International Mechanical Engineering Congress and Exposition*, IMECE2004-59727, 2004.

[8] E.J. Barth, M.A. Gogola, and M. Goldfarb, "Modeling and Control of a Monopropellant-Based Pneumatic Actuation System," *Proceedings of 2003 IEEE International Conference on Robotics and Automation,* Vol. I, pp. 628-633, 2003.

[9] B. Khoumeri, N. Balbi, E. Leoni, N. Chiaramonti, and J. H. Balbi, "The Decomposition of Hydrogen Peroxide – A Non-linear Dynamic Model", *Journal of Thermal Analysis and Calorimetry*, Vol. 59, pp. 901-911, 2000.

Table 1. Controller parameters.

PARAMETER	VALUE
k	380 kJ/kg
τ_R	0.001 s
T_{ADT}	505 K
ρ_L	1290 kg/m^3
C_P	1620 J/kg/K
γ	1.34
R	408 J/kg/K
c	0.13
C_F	0.29
C_R	0.54
$A_{V,IN,MAX}$	1.4 mm^2
$A_{V,EX,MAX}$	16 mm^2
λ	80 rad/s
Φ	400 kN/s
K	0.03 mm^2

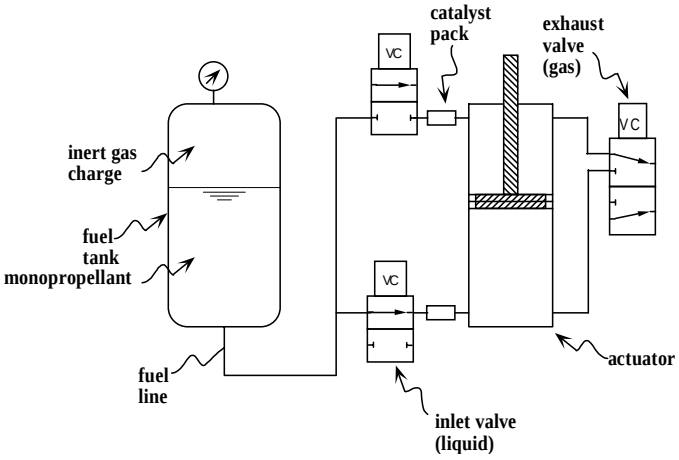

Fig. 1. Schematic of the proportional injector direct-injection (PIDI) monopropellant-powered actuation system.

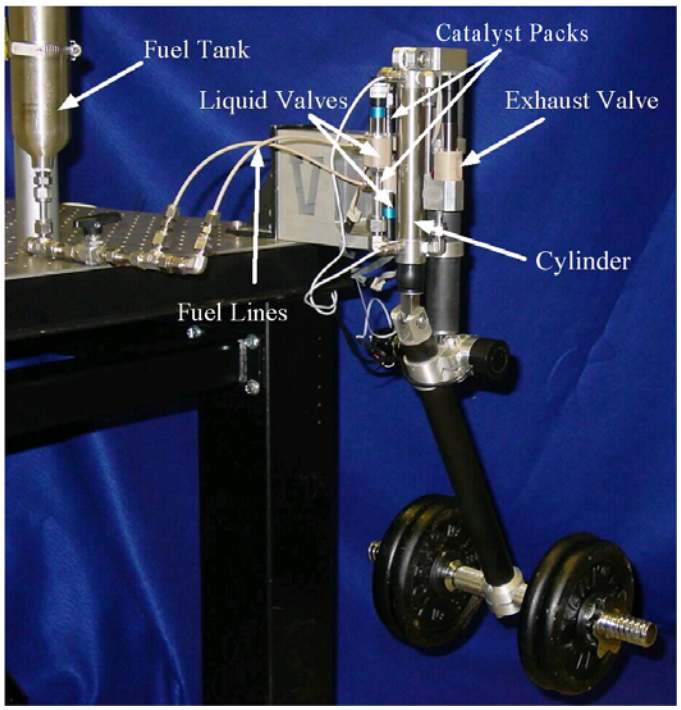

Fig. 2. PIDI actuator integrated with a single-DOF robot arm.

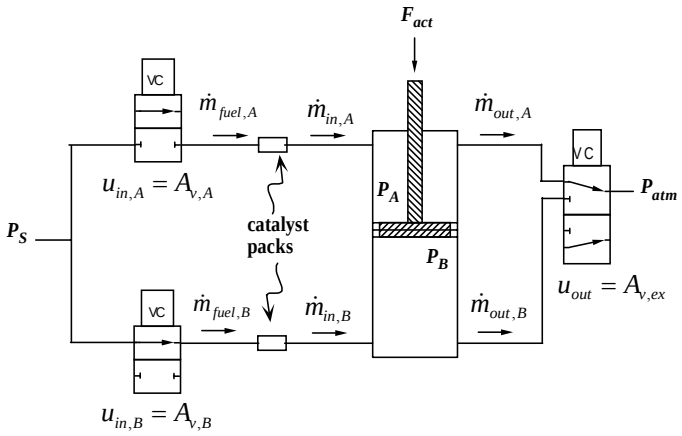

Fig. 3. Modeling schematic of the PIDI actuator.

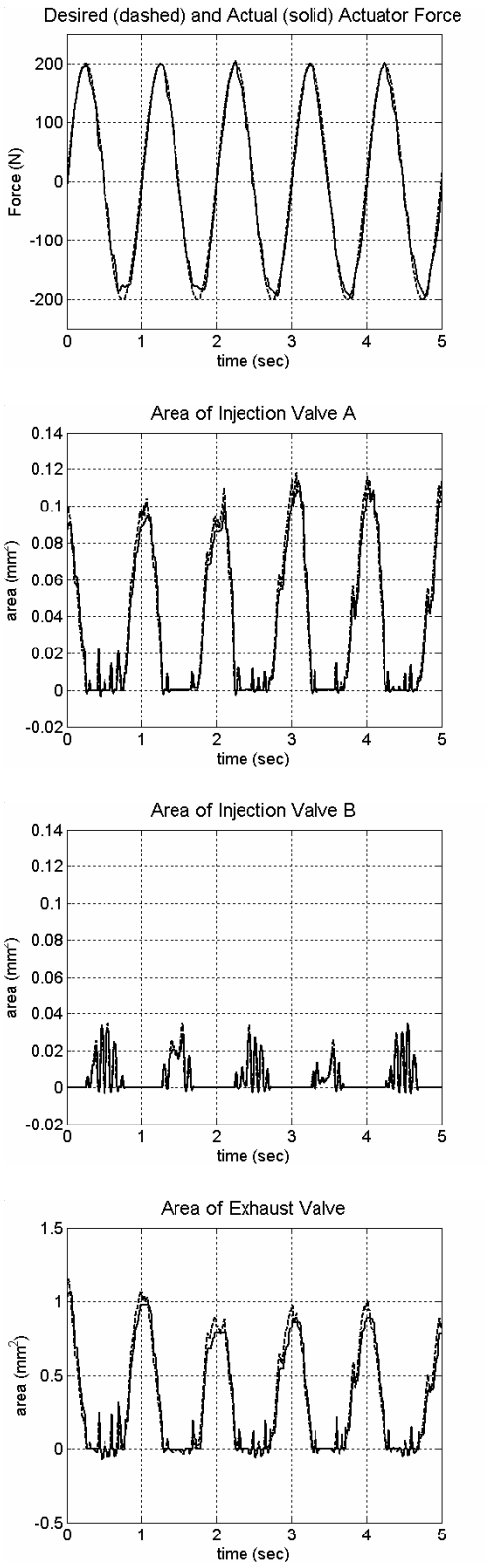

Fig. 4. Sinusoidal force tracking of the PIDI monopropellant-powered actuator at a frequency of 1 Hz, and corresponding valve commands.

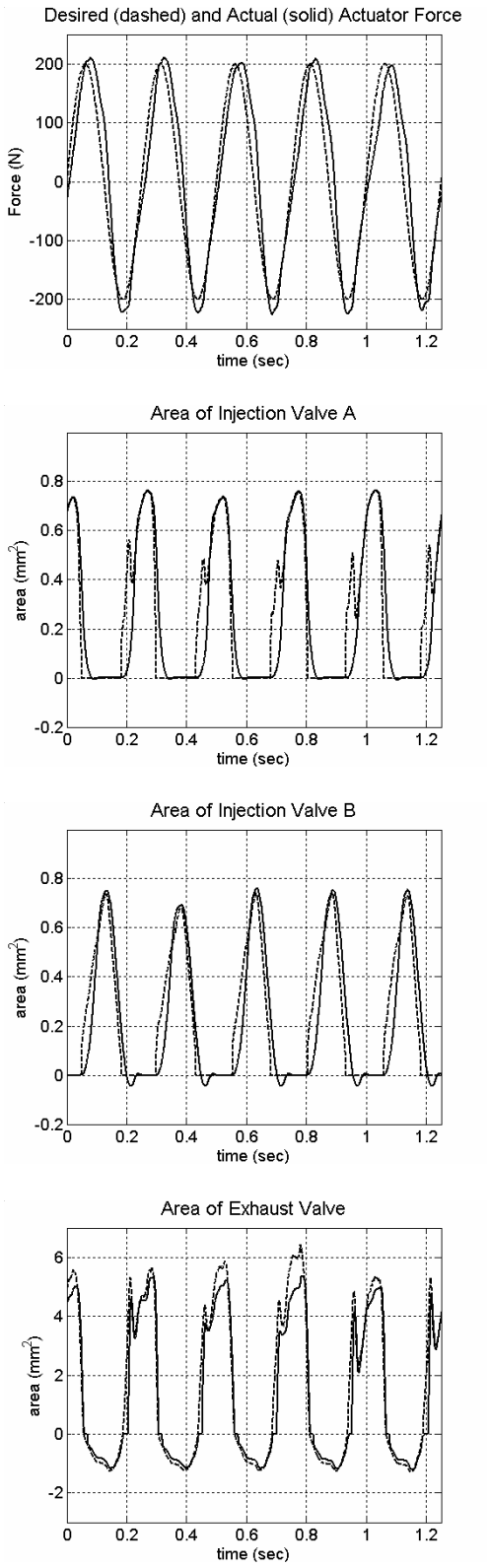

Fig. 5. Sinusoidal force tracking of the PIDI monopropellant-powered actuator at a frequency of 4 Hz, and corresponding valve commands.

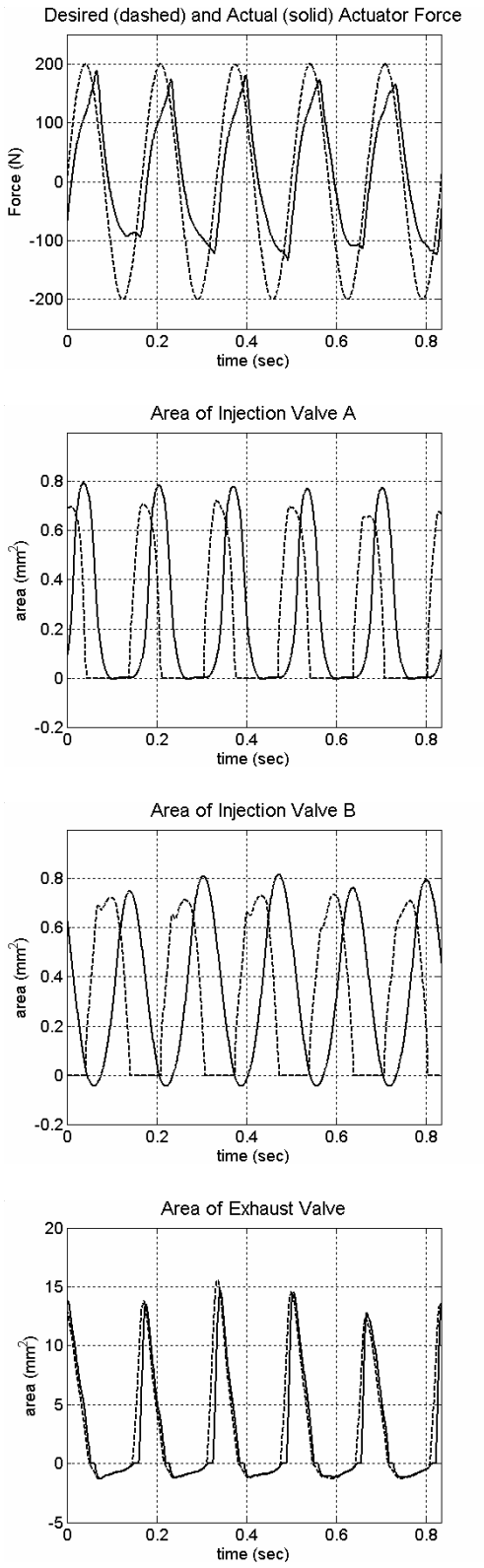

Fig. 6. Sinusoidal force tracking of the PIDI monopropellant-powered actuator at a frequency of 6 Hz, and corresponding valve commands.